HHS Public Access

Author manuscript

Nature. Author manuscript; available in PMC 2012 December 25.

Published in final edited form as:

Nature. ; 482(7386): 552–556. doi:10.1038/nature10867.

Structure and Dynamics of the M_3 Muscarinic Acetylcholine Receptor

Andrew C. Kruse[1], **Jianxin Hu**[2], **Albert C. Pan**[3], **Daniel H. Arlow**[3], **Daniel M. Rosenbaum**[4], **Erica Rosemond**[2], **Hillary F. Green**[3], **Tong Liu**[2], **Pil Seok Chae**[5], **Ron O. Dror**[3], **David E. Shaw**[3], **William I. Weis**[1,6], **Jurgen Wess**[2,*], and **Brian Kobilka**[1,*]

[1]Department of Molecular and Cellular Physiology, Stanford University School of Medicine, Stanford, California 94305, USA

[2]Molecular Signaling Section, Laboratory of Bioorganic Chemistry, National Institute of Diabetes and Digestive and Kidney Diseases, Bethesda, Maryland 20892, USA

[3]D. E. Shaw Research, New York, New York 10036, USA

[4]Department of Biochemistry, University of Texas Southwestern Medical Center, Dallas, Texas 75390, USA

[5]Department of Bionano Engineering, Hanyang University, Ansan 426-791, Korea

[6]Department of Structural Biology, Stanford University School of Medicine, 299 Campus Drive, Stanford, California 94305, USA

Abstract

Acetylcholine (ACh), the first neurotransmitter to be identified[1], exerts many of its physiological actions via activation of a family of G protein-coupled receptors (GPCRs) known as muscarinic ACh receptors (mAChRs). Although the five mAChR subtypes (M_1-M_5) share a high degree of sequence homology, they show pronounced differences in G protein coupling preference and the physiological responses they mediate.[2–4] Unfortunately, despite decades of effort, no therapeutic agents endowed with clear mAChR subtype selectivity have been developed to exploit these

*Correspondence and requests for materials should be addressed to B.K.K. (kobilka@stanford.edu) or J.W. (jwess@helix.nih.gov).

Author Contributions A.C.K cloned, expressed, and purified several M_3 receptor crystallization constructs; developed the purification procedure; performed crystallization trials, collected diffraction data, solved and refined the structure. J.H. prepared, expressed, and characterized various M_3 receptor constructs in ligand binding and functional assays. A.C.P. and D.H.A. designed, performed, and analyzed molecular dynamics (MD) simulations and assisted with manuscript preparation. D.M.R. assisted in design and characterization of initial M_3-T4L fusion constructs. E.R. prepared, expressed, and tested the pharmacology and stability of several M_3 receptor-T4 fusion constructs in insect cells. H.F.G. analyzed MD simulations and crystallographic data and assisted with manuscript preparation. T.L. performed binding assays and functional experiments together with J.H. P.S.C. developed and prepared neopentyl glycol detergents used for purifying the M_3 receptor. R.O.D. oversaw, designed, and analyzed MD simulations. D.E.S. oversaw MD simulations and analysis. W.I.W. oversaw refinement of the M_3 receptor structure, and assisted in analysis of diffraction data. J.W. provided advice regarding construct design, protein expression, and project strategy; oversaw initial insect cell expression and pharmacological and functional characterization of M_3 receptor constructs. B.K.K. was responsible for overall project strategy; guided design of crystallization constructs; assisted with crystal harvesting and data collection. A.C.K., R.O.D., J.W., and B.K.K. wrote the manuscript.

Coordinates and structure factors for M_3-T4L are deposited in the Protein Data Bank (accession code 4DAJ)

The authors declare no competing financial interests

differences.[5–6] We describe here the structure of the $G_{q/11}$-coupled M_3 mAChR bound to the bronchodilator drug tiotropium and identify the binding mode for this clinically important drug. This structure, together with that of the $G_{i/o}$-coupled M_2 receptor, offers new possibilities for the design of mAChR subtype-selective ligands. Importantly, the M_3 receptor structure allows the first structural comparison between two members of a mammalian GPCR subfamily displaying different G-protein coupling selectivities. Furthermore, molecular dynamics simulations suggest that tiotropium binds transiently to an allosteric site *en route* to the binding pocket of both receptors. These simulations offer a structural view of an allosteric binding mode for an orthosteric GPCR ligand and raise additional opportunities for the design of ligands with different affinities or binding kinetics for different mAChR subtypes. Our findings not only offer new insights into the structure and function of one of the most important GPCR families, but may also facilitate the design of improved therapeutics targeting these critical receptors.

The mAChR family consists of five subtypes, M_1-M_5, which can be subdivided into two major classes (Fig 1a). The M_1, M_3, and M_5 receptors show selectivity for G proteins of the $G_{q/11}$ family, whereas the M_2 and M_4 receptors preferentially couple to $G_{i/o}$-type G proteins[2–4]. The development of small molecule ligands that can selectively act on specific mAChR subtypes has proven extremely challenging, primarily due to the high degree of sequence similarity in the transmembrane (TM) core of these receptors[2–4]. More recently, considerable progress has been made in targeting drugs to non-classical (allosteric) binding sites of certain mAChR subtypes[5].

Within the mAChR family, the M_3 subtype mediates many important physiological functions, including smooth muscle contraction and glandular secretion[3,4,6–9]. Central M_3 receptors have also been implicated in the regulation of food intake[7], learning and memory[8], and the proper development of the anterior pituitary gland[9]. Selective drugs targeted at this receptor subtype may prove clinically useful[4,6–9], and non-selective muscarinic ligands are already widely used in current practice.

Due to the profound physiological importance of the M_3 receptor and its longstanding role as a model system for understanding GPCR function[3,10], we used the T4 lysozyme (T4L) fusion protein strategy[11] to obtain crystals of *Rattus norvegicus* M_3 receptor-T4L fusion protein (Supplementary Fig. 1) by lipidic cubic phase crystallization. Diffraction data from more than 70 crystals were merged to create a data set to 3.4 A resolution and to solve the structure by molecular replacement. The M_3 receptor structure, together with that of the M_2 receptor[12], affords for the first time an opportunity to compare two closely related mammalian receptors with divergent G protein coupling selectivities.

The overall structure of the M_3 receptor is similar to that of M_2 (Fig. 1b-d). Surprisingly, structural conservation includes intracellular loops (ICLs) 1 and 2, and extracellular loops (ECLs) 1–3, which share highly similar overall folds despite low sequence conservation (Fig. 1f). Like the M_2 receptor, the M_3 receptor exhibits unique mAChR features, including a large extracellular vestibule as part of an extended hydrophilic channel containing the orthosteric binding site (Fig. 1e). Also like M_2, the M_3 receptor features a pronounced outward bend at the extracellular end of TM4 (Fig. 1d; Supplementary Fig. 2b). This bend, not seen in any other GPCR family crystallized to date, is stabilized by a hydrogen bond

from the Q207 (Q163 in M_2) side chain to the L204 backbone peptide carbonyl (Supplementary Fig. 2b). This bond is part of a polar interaction network involving four residues absolutely conserved within the mAChR family, suggesting that this unusual feature is important to mAChRs in general. Indeed, mutagenesis of Q207 in M_3 impaired both ligand binding and receptor activation[13].

The M_3 receptor was crystallized in complex with tiotropium (Spiriva), a potent muscarinic inverse agonist[14,15] used clinically for the treatment of chronic obstructive pulmonary disease. The M_2 receptor was crystallized in complex with R-(–)-3-quinuclidinyl benzilate (QNB) which, like tiotropium, is a non-subtype-selective mAChR blocker[14,16]. The two ligands bind in remarkably similar poses (Fig. 2b), and it is likely that this pose represents a conserved binding mode for structurally similar anticholinergics. In the M_3 receptor, as in M_2, the ligand is deeply buried within the TM receptor core (Fig. 2a, d) and is covered by a lid comprised of three conserved tyrosines, $Y148^{3.33}$, $Y506^{6.51}$, and $Y529^{7.39}$ (Fig. 2a; superscripts indicate Ballesteros-Weinstein numbers[17]). The ligand is almost completely occluded from solvent and engages in extensive hydrophobic contacts with the receptor. A pair of hydrogen bonds are formed from $N507^{6.52}$ to the ligand carbonyl and hydroxyl, while $D147^{3.32}$ interacts with the ligand amine.

Reflecting the difficulty in developing subtype-selective orthosteric ligands, the residues forming the orthosteric binding pocket are absolutely conserved among the five mAChR subtypes (Fig. 1f). However, this conservation at the amino acid level does not preclude the existence of differences in the three-dimensional architecture of the orthosteric site between the different mAChR subtypes. In fact, comparison of the structures of the M_3 and M_2 receptor ligand binding sites reveals for the first time structural divergences that might be exploited in the development of subtype-selective ligands.

One such difference derives from the replacement of Phe181 in ECL2 of M_2 with Leu225 in M_3 (this residue is leucine in all mAChRs except M_2). This creates a pocket in M_3 not found in M_2 (Fig. 2c,d). A second difference is a 2.8 A shift of $Tyr529^{7.39}$ relative to the position of the corresponding M_2 residue (Tyr426; Fig. 2e). This feature may derive from a difference in the identity of the residue in position 2.61 (Phe124 in M_3 and Tyr80 in M_2; Fig. 2f). This residue interacts directly with TM7, influencing the position of this helix and the residues within it, including $Tyr529^{7.39}$. Notably, the residue at position 2.61 is not a part of the orthosteric binding pocket, but is positioned near a probable allosteric binding site[12]. Since tiotropium and QNB are structurally similar but not identical, the observed binding site differences must be interpreted with some degree of caution. However, site-directed mutagenesis studies with M_1 and M_3 receptors support the concept that the residue at position 2.61 plays a role in receptor activation[18,19], and ligand binding selectivity[20]. This site does not appear to play a role in determining antagonist dissociation rates, since mutation of M_3 $F^{2.61}$ to tyrosine or of M_2 $Y^{2.61}$ to phenylalanine had no effect on dissociation rates for [^{3}H]NMS or [^{3}H]QNB.

We used molecular dynamics simulations to characterize the pathway by which tiotropium binds to and dissociates from the M_2 and M_3 receptors. Similar techniques have previously been shown to correctly predict crystallographic ligand binding poses and kinetics in studies

of β-adrenergic receptors[21]. In both the M_2 and M_3 receptors, our simulations indicate that as tiotropium binds to or dissociates from the receptor, it pauses at an alternative binding site in the extracellular vestibule (Fig. 3, Supplementary Fig. 3). Intriguingly, this site corresponds to an allosteric site that has been previously identified by mutagenesis[12], a finding consistent with pharmacological studies showing that orthosteric ligands can act as allosteric modulators at the M_2 receptor[22].

Tiotropium adopts different preferred allosteric binding poses in M_2 and M_3 (Fig. 3d, Supplementary Fig. 4). These metastable binding poses, which appear independently in both binding and dissociation simulations, may represent the first structural view of a clinically used “orthosteric” GPCR ligand binding to an experimentally validated allosteric site. Conceivably, therapeutic molecules could be rationally engineered to act independently as both allosteric and orthosteric ligands (in contrast to previously described bitopic ligands that bind at both sites simultaneously[23]). Tiotropium dissociates from M_3 receptors more slowly than from M_2 receptors, a phenomenon thought to provide clinically important “kinetic selectivity” of this drug for M_3 receptors despite similar equilibrium binding affinities for both subtypes[14]. In simulations with tiotropium bound, the portion of ECL2 nearest the binding pocket proved more mobile in M_2 than in M_3 (Supplementary Fig. 5), likely due to multiple sequence differences between the two receptor subtypes. This increased mobility disrupts a hydrophobic cluster involving a thiophene ring of tiotropium, the ECL2 residue Phe181(M_2)/Leu225(M_3), and Tyr$^{3.33}$, facilitating movement of Phe181/Leu225 away from the orthosteric site and rotation of Tyr$^{3.33}$ toward TM4. In simulations of ligand dissociation, such motions clear a path for tiotropium’s egress from the orthosteric site to the extracellular vestibule. The increased mobility of ECL2 in M_2 thus appears to facilitate tiotropium’s traversal of the largest energetic barrier on the binding/dissociation pathway (Fig. 3c). Experimental measurements with wild-type and mutant receptors (M_3 L225F and M_2 F181L) suggest that the Leu225/Phe181 sequence difference alone is insufficient to explain the difference in off-rates, (for practical reasons these measurements were performed with QNB rather than tiotropium; see Online Methods).

One of the most interesting features of the M_2 and M_3 receptors is the fact that the two highly similar receptors display pronounced differences in G-protein coupling specificity. For this reason, the M_2/M_3 receptor pair has long served as an excellent model system to identify features contributing to GPCR-G protein coupling selectivity[3]. Since no simple sequence elements have been identified as general determinants of coupling specificity across GPCR families[24], it is likely that recognition depends on features such as overall conformation in addition to specific inter-residue contacts.

The M_2 and M_3 receptor structures show a significant difference in the position of the cytoplasmic end of TM5 and of ICL2 (Fig. 4a, b). The highly conserved tyrosine residue at position 5.58 (M_3 Tyr250$^{5.58}$, M_2 Tyr206$^{5.58}$) shows a clear deviation between the two receptors, pointing toward the core of the protein in M_2, and away from the receptor toward the surrounding lipid bilayer in M_3. Interestingly, mutagenesis studies have identified a tetrad of residues (‘AALS’ in M_3, ‘VTIL’ in M_2) located on the cytoplasmic end of TM6 that are critical in determining G protein coupling selectivity[25,26]. In both structures, these residues interact directly with TM5 (Fig. 4a), and in the β_2 adrenergic receptor-G_s

complex[27] two of the four corresponding residues make contact with the carboxy terminal helix of $G\alpha_s$. M_3 Tyr254$^{5.62}$ at the bottom of TM5 also plays a role in activation of $G_{q/11}$[28]. In the M_2 receptor structure, the corresponding residue (Ser210$^{5.62}$) is displaced by approximately 4 A relative to Tyr254$^{5.62}$ in M_3 (Fig. 4a).

When we compared the position of TM5 in the M_2 and M_3 receptors to that in other GPCR structures, we found that it is M_2-like in all $G_{i/o}$-coupled receptors, while the two mammalian $G_{q/11}$-coupled receptors solved to date exhibit another conformation (Fig. 4c, d). An important caveat here is that these structures have been solved using the T4L fusion strategy, and we cannot completely exclude the possibility that this approach perturbs the conformation of TMs 5 and 6. However, in molecular dynamics simulations of M_2 and M_3 receptors without T4L, each of the receptors adopts a set of conformations that includes its own crystallographically observed conformation (Supplementary Fig. 6, 7). These simulations suggest that the observed conformations are unlikely to be artifacts of the crystallization methodology, though the crystal structures likely represent only one conformation among many adopted by the receptors in a biological context.

The structure of the M_3 receptor, together with that of the M_2 receptor[12], offers a unique opportunity to directly compare the structural properties of two members of a mammalian GPCR subfamily endowed with different G-protein coupling selectivities. Examination of the M_3 structure has provided the first structural evidence of differences between ligand binding sites of mAChR subtypes that could be exploited for the design of more selective therapeutics. Moreover, computational studies have identified a pathway by which the COPD drug tiotropium may bind to and dissociate from the M_3 receptor, offering the first structural view of an orthosteric GPCR ligand binding to an experimentally validated allosteric site. This information should facilitate the rational design of new muscarinic drugs exhibiting increased receptor subtype selectivity, potentially improving treatment for a wide variety of important clinical disorders.

Methods summary

The M_3 muscarinic receptor-T4 lysozyme fusion protein was expressed in Sf9 insect cells and purified by nickel affinity chromatography followed by FLAG antibody affinity chromatography and then size exclusion chromatography. It was crystallized using the lipidic cubic phase technique, and diffraction data were collected at the GM/CA-CAT beamline at the Advanced Photon Source at Argonne National Lab. The structure was solved by molecular replacement using merged data from 76 crystals. All-atom classical molecular dynamics simulations with explicitly represented lipids and water were performed using the CHARMM force field[29] on Anton[30]. Ligand-binding simulations included no artificial forces. Dissociation studies included a time-varying biasing term that gradually forces the ligand away from its crystallographic position, but not along any prespecified pathway or direction. Full details are provided in the online methods.

Online Methods

Expression and purification of M_3 muscarinic receptor

The wild-type M_3 mAChR contains several long, likely poorly ordered regions, including the extracellular amino terminal domain and the third intracellular loop, making it a challenging candidate for crystallographic studies. To alleviate this problem, the M_3 receptor from *Rattus Norvegicus* was modified to include a TEV protease recognition site in the amino terminus and a hexahistidine tag at the carboxy terminus. Moreover, the third intracellular loop (residues 260–481) was replaced with T4 lysozyme residues 1-161 in a manner described previously[11], with two different fusions tested. These modifications are diagrammed in figure S1, which also shows the final crystallization construct.

The pharmacological properties of the construct were tested and compared to those of the wild-type receptor (Fig. S8, supplementary table 1; see below for methods details). Both constructs showed almost identical affinity for antagonists, while the crystallization construct (M_3-crys) showed somewhat higher affinity for the agonist acetylcholine than the wild-type construct. A similar observation has been noted previously in the β_2 adrenergic receptor[11]. Studies with membranes prepared from transfected COS-7 cells showed that TEV cleavage of M_3-crys (to remove most of the N-terminal tail) had no significant effect on ligand binding affinities (Fig. S9). Moreover, the wild-type receptor and M_3-crys, either cleaved with TEV or left uncleaved, showed very similar [^{3}H]-QNB dissociation rate kinetics (Fig. S10). As expected, the crystallization construct failed to stimulate agonist-dependent phosphoinositide hydrolysis in transfected COS cells (data not shown), likely because essential G protein interacting regions in intracellular loop 3 were omitted from the construct and also because the T4 lysozyme fusion protein sterically blocks G protein association.

The crystallization construct was expressed in Sf9 cells using the baculovirus system in the presence of 1 μM atropine. M_3 receptors expressed in Sf9 cells are known to exhibit functional and pharmacological properties similar to M_3 receptors expressed in mammalian cells[31]. Infection was performed at 4×10^6 cells per mL and flasks were shaken at 27 °C for 60 hr following infection.

Cells were harvested by centrifugation, then lysed by osmotic shock in the presence of 1 μM tiotropium bromide (obtained from W & J PharmaChem, Inc., Silver Spring, MD, USA), which was present in all subsequent buffers. Receptor was extracted from cells using a dounce homogenizer with a buffer of 0.75 M NaCl, 1% dodecyl maltoside (DDM), 0.03% cholesterol hemisuccinate (CHS), 30 mM HEPES pH 7.5, and 30% glycerol. Iodoacetamide (2 mg/mL) was added to block reactive cysteines at this stage. Nickel-NTA agarose was added to the solubilized receptor without prior centrifugation, stirred for two hr, and then washed in batch with 100 × g spins for 5 min each. Washed resin was poured into a glass column, and receptor was eluted in 0.1% DDM, 0.03% CHS, 20 mM HEPES pH 7.5, 0.75 M NaCl, and 250 mM imidazole.

Nickel resin-purified receptor was then loaded by gravity flow over anti-FLAG M1 affinity resin. Following extensive washing, detergent was gradually exchanged over 1.5 hr into a

buffer in which DDM was replaced with 0.01% lauryl maltose neopentyl glycol (MNG), and the NaCl concentration was lowered to 100 mM. MNG has been shown to be more effective at stabilizing muscarinic receptors than DDM[32]. Receptor was eluted with 0.2 mg/mL FLAG peptide and 5 mM EDTA. TEV protease (1:10 w/w) was added and incubated with receptor for 1.5 hr at room temperature to remove the flexible amino terminal tail. Receptor was then separated from TEV by size exclusion chromatography (SEC) on a Sephadex S200 column (GE Healthcare) in a buffer of 0.01% MNG, 0.001% CHS, 100 mM NaCl, and 20 mM HEPES pH 7.5. Tiotropium was added to a final concentration of 10 μM following SEC. The resulting receptor preparation was pure and monomeric (Fig. S11). Purification of unliganded M_3 receptor was also possible by this procedure, but the resulting preparation was polydisperse and unsuitable for crystallographic study.

Crystallization and data collection

Purified M_3 receptor was concentrated to 60 mg/mL, then mixed with 1.5 parts by weight of a 10:1 mix of monoolein with cholesterol (Sigma) using the two syringe reconstitution method[33]. The resulting lipidic cubic phase mix was dispensed in 15 nL drops onto glass plates and overlaid with 600 nL precipitant solution using a Gryphon LCP robot (Art Robbins Instruments). Crystals grew after 2 - 3 days in precipitant solution consisting of 27 – 38 % PEG 300, 100 mM HEPES pH 7.5, 1 % (w/w) 1,2,3-heptanetriol, and 100 mM ammonium phosphate. Typical crystals are shown in figure S12.

Data collection was performed at Advanced Photon Source GM/CA-CAT beamlines 23ID-B and 23ID-D using a beam size of 5 or 10 microns for most crystals. Diffraction quality rapidly decayed following exposure, and wedges of typically 5 degrees were collected and merged from 76 crystals using HKL2000[34]. Diffraction quality ranged from 3–4 A in most cases, with strong anisotropy evident in many frames. Most crystals tested showed evidence of epitaxial twinning, though in most cases one of the two twins dominated the observed diffraction pattern, allowing processing as a single crystal. A more extensive discussion of the twinning is given below. Some contamination of diffraction measurements due to the twin-related reflections was unavoidable, leading to slightly poorer merging statistics than is typical for datasets collected from many small crystals (Supplementary table 2). Despite this, maps were generally of high quality and electron density was easily interpretable (Figs. S13, S14), in part due to the availability of non-crystallographic symmetry.

Analysis of $\langle F \rangle / \langle \sigma F \rangle$ along each of the three reciprocal space axes indicated that the diffraction was strong in two directions, and weak in the third direction, along the reciprocal space axis c^* (Fig. S15). Using $\langle F \rangle / \langle \sigma F \rangle$ greater than 3 as a guideline suggested a resolution cutoff of better than 3.2 A along a^* and b^*, and of 4.0 A along c^*. We therefore applied an ellipsoidal truncation along these limits, and then applied an overall spherical truncation at 3.4 A due to low completeness in higher resolution shells. Fortunately, 4-fold non-crystallographic symmetry (NCS) allowed for improved map quality with map sharpening followed by NCS averaging, largely alleviating the effects of anisotropic diffraction and epitaxial twinning to give highly interpretable maps (Fig. S13, S14) and allowing details of ligand recognition to be clearly resolved (Supplementary table 3).

The structure of the M_3 receptor was solved using the structure of the M_2 muscarinic receptor (companion manuscript) as the search model in Phaser[35]. The model was improved through iterative refinement in Phenix[36] and manual rebuilding in Coot guided by both NCS averaged and unaveraged maps. NCS restraints were applied in initial refinement stages, and omitted in final refinement cycles to account for differences between NCS-related copies. The quality of the resulting structure was assessed using MolProbity[37], and figures were prepared using PyMOL[38].

Epitaxial twinning

Crystals of the M_3 receptor showed hallmarks of epitaxial twinning, such as mixed sharp and split spots, poor indexing, and many unpredicted reflections in some frames. In some cases diffraction from two distinct lattices was clearly visible, with a small fraction of reflections exactly superimposed from both lattices (Fig. S16). In most cases one lattice dominated the diffraction pattern to such an extent that it could be easily processed as a single crystal. Intriguingly, the two indexing solutions were not equivalent cells but rather were two enantiomorphic P1 cells (supplementary table 2).

As one of these two cells gave significantly better diffraction data than the other, data processing and refinement were only pursued in this case. Within the asymmetric unit, two layers of receptors and two layers of T4 lysozyme are present, but each of these four layers exhibits a different lattice packing (Fig. S17, S18). The order in which these layers are stacked in the crystal defines a unique direction along *c*, the axis normal to the membrane plane. Since P1 is a polar space group, the positive direction along *c* is uniquely defined, and the two possible orientations of the stacked layers of membrane relative to the positive direction along *c* distinguish the two twin crystal forms.

Transient expression of wild-type and modified M_3 receptors in COS-7 cells, membrane preparation, and TEV treatment

COS-7 cells were cultured as described previously[39]. About 24 h prior to transfections, ~1 × 10^6 cells were seeded into 100 mm dishes. Cells were transfected with 4 μg/dish of receptor plasmid DNA using the Lipofectamine Plus kit (Invitrogen, Carlsbad, CA), according to the manufacturer's instructions. The mammalian expression plasmid coding for the wild type rat M_3 receptor has been described previously[40]. The coding sequence of the modified M_3 receptor construct used for crystallization studies (M_3-crys; see Fig. S8, supplementary table 1) was inserted into the pcDNA3.1(-) vector. Transfected cells were incubated with 1 μM atropine for the last 24 h of culture to increase receptor expression levels[39]. COS-7 cells were harvested ~48 h after transfections, and membranes were prepared as described in detail by Ward *et al.*[39]

Membranes prepared from COS-7 cells transiently expressing M_3-crys were resuspended in TEV protease digestion buffer (50 mM NaCl, 10 mM HEPES pH 7.5, and 1 mM EDTA) and incubated overnight with TEV protease (homemade, final concentration: 1 μM) at 4 ůC with rotation. Efficient removal of the N-terminal tail of Mů-crys by TEV was confirmed by SDS-PAGE and immunoblotting using a monoclonal anti-FLAG antibody directed against the N-terminus of M_3-crys. TEV-treated membranes were resuspended in either buffer A (25

mM sodium phosphate and 5 mM $MgCl_2$, pH 7.4) for radioligand binding studies or in sodium- potassium-phosphate buffer (4 mM Na_2HPO_4, 1 mM KH_2PO_4, pH 7.4) for [^{3}H]QNB dissociation assays (see below).

Radioligand binding studies

[^{3}H]*N*-methylscopolamine ([^{3}H]NMS) saturation and competition binding studies were carried out essentially as described previously[41]. In brief, membrane homogenates prepared from transfected COS-7 cells (~10 20 μg of membrane protein per tube) were incubated with the muscarinic antagonist/inverse agonist, [^{3}H]NMS, for 3 h at 22 °C in 0.5 ml of binding buffer containing 25 mM sodium phosphate and 5 mM $MgCl_2$ (pH 7.4). In saturation binding assays, we employed six different [^{3}H]NMS concentrations ranging from 0.1 to 6 nM. In competition binding assays, we studied the ability of tiotropium, atropine, or acetylcholine to interfere with [^{3}H]NMS (0.5 nM) binding. Incubations were carried out for 20 hr in the case of tiotropium in order to achieve equilibrium binding[42] (3 hr for all other ligands). Nonspecific binding was assessed as binding remaining in the presence of 1 μM atropine. Binding reactions were terminated by rapid filtration over GF/C Brandel filters, followed by three washes (~4 ml per wash) with ice-cold distilled water. The amount of radioactivity that remained bound to the filters was determined by liquid scintillation spectrometry. Ligand binding data were analyzed using the nonlinear curve-fitting program Prism 4.0 (GraphPad Software Inc., San Diego, CA).

Atropine sulfate and acetylcholine chloride were from Sigma-Aldrich (St. Louis, MO). Tiotropium bromide was purchased from W&J PharmaChem, Inc. (Silver Spring, MD). [^{3}H]NMS (specific activity: 85.0 Ci/mmol) was obtained from PerkinElmer Life Sciences (Waltham, MA).

[^{3}H]-QNB dissociation rate assays

[^{3}H]-QNB (PerkinElmer; specific activity: 50.5 Ci/mmol) dissociation rate assays were carried out as described previously[43]. Measurements were carried out at 37 °C in a total volume of 620 μl using a buffer consisting of 4 mM Na_2HPO_4 and 1 mM KH_2PO_4 (pH 7.4). Membranes prepared from transfected COS-7 cells (final protein concentration: 10 μg protein/ml) were prelabeled with 1 nM [^{3}H]-QNB for 30 min. Dissociation of the labeled ligand was initiated by the addition of atropine (final concentration: 3 μM). Incubations were terminated by filtration through GF/C Brandel fiber filters that had been pretreated with 0.1% polyethyleneimine, followed by two rinses with ice-cold distilled water. The amount of radioactivity that remained bound to the filters was determined by liquid scintillation spectrometry.

Molecular dynamics

In all simulations, the receptor was embedded in a hydrated lipid bilayer with all atoms, including those in the lipids and water, represented explicitly. Simulations were performed on Anton[30], a special-purpose computer designed to accelerate standard molecular dynamics simulations by orders of magnitude.

System setup and simulation protocol

Simulations of the M_2 receptor were based on the crystal structure of the QNB–M_2 complex, and simulations of M_3 were based on the structure of the tiotropium–M_3 complex (chain A). These crystal structures were determined using a T4 lysozyme (T4L) fusion strategy, in which intracellular loop 3 (ICL3) of each receptor was replaced by T4L; the T4L sequence was omitted in our simulations. All chain termini were capped with neutral groups (acetyl and methylamide). Residues 6.31–6.33 near the intracellular end of TM6 were unresolved in the M_3 crystal structure, and residues 6.27–6.30 were resolved in an unstructured conformation packed against T4L. Residues 6.27–6.36 were modeled manually as a helical extension of TM6, with side chains then placed using Prime. Hydrogens were added to the crystal structures using Maestro (Schrodinger LLC, New York, NY), as described in previous work[44]. All titratable residues were left in the dominant protonation state at pH 7.0, except for Asp69$^{2.50}$ in M_2 and Asp114$^{2.50}$ in M_3, which were protonated. Asp69$^{2.50}$ and Asp114$^{2.50}$ correspond to rhodopsin Asp83$^{2.50}$, which is protonated during the entire photocycle[45].

Prepared protein structures were inserted into an equilibrated POPC bilayer as described in previous work[46]. Sodium and chloride ions were added to neutralize the net charge of the system and to create a 150 mM solution.

Simulations of the M_3 receptor initially measured 80 × 80 × 87 A^3 and contained 163 lipid molecules, 26 sodium ions, 41 chloride ions, and approximately 9,897 water molecules, for a total of ~56,000 atoms. Simulations of the M_2 receptor initially measured 79 × 79 × 85 A^3 and contained 156 lipid molecules, 24 sodium ions, 35 chloride ions, and approximately 9,165 water molecules, for a total of ~53,000 atoms. To simulate M_2 with tiotropium bound, we removed the co- crystallized ligand, QNB, and docked in tiotropium using Glide (Schrodinger LLC, New York, NY).

All simulations were equilibrated using Anton in the NPT ensemble at 310 K (37 °C) and 1 bar with 5 kcal mol $^1A^2$ harmonic position restraints applied to all non-hydrogen atoms of the protein and the ligand (except for the tiotropium–M_2 complex, where the ligand was unrestrained); these restraints were tapered off linearly over 50 ns. All bond lengths to hydrogen atoms were constrained using M-SHAKE[47]. A RESPA integrator[48] was used with a time step of 2 fs, and long-range electrostatics were computed every 6 fs. Production simulations were initiated from the final snapshot of the corresponding equilibration runs, with velocities sampled from the Boltzmann distribution at 310 K, using the same integration scheme, long-range electrostatics method, temperature, and pressure. Van der Waals and short-range electrostatic interactions were cut off at 13.5 A and long-range electrostatic interactions were computed using the *k*-space Gaussian Split Ewald method[49] with a 32 × 32 × 32 grid, σ = 3.33 A, and σ_s = 2.33 A.

Spontaneous binding of tiotropium and acetylcholine

We performed simulations where tiotropium was placed arbitrarily in the bulk solvent (at least 40 A from the entrance to the extracellular vestibule) and allowed to diffuse freely until it associated spontaneously with the M_2 or M_3 receptor, following methodology described in

previous work[21]. In these simulations (Supplementary table 4, conditions D and E), the co-crystallized ligand was removed and four tiotropium molecules were placed in the bulk solvent. A tiotropium molecule bound to the extracellular vestibule at least once in each simulation. In the longer simulations, tiotropium bound to and dissociated from the extracellular vestibule multiple times. Tiotropium assumed several different poses when bound to the extracellular vestibule of either M_2 or M_3 (Fig. S4). Tiotropium never entered the orthosteric binding pocket, presumably because the simulations were not of sufficient length.

The fact that tiotropium associated with and dissociated from the vestibule multiple times, but did not enter the binding pocket, suggests that tiotropium must traverse a larger energetic barrier to enter the binding pocket of M_2 or M_3 from the extracellular vestibule than to enter the vestibule from bulk solvent. This contrasts with earlier simulations on alprenolol binding to the β_2-adrenergic receptor, in which the largest energetic barrier (by a small margin) was between the bulk solvent and the extracellular vestibule[21]. This difference likely reflects the fact that ligands must pass through a much tighter passageway to enter the binding pocket of the M_2 and M_3 receptors from the vestibule than is the case for the β_2-adrenergic receptor. Tiotropium lost the majority of its hydration shell as it entered the vestibule (Fig. S19), as observed previously for ligands binding to β-adrenergic receptors[21].

We followed a similar protocol in a simulation of the M_3 receptor in the presence of the agonist acetylcholine, a smaller molecule which might be expected to bind faster (Supplementary table 4, condition F). Indeed, an acetylcholine molecule bound in the orthosteric binding pocket after 9.5 μs and remained there for the remainder of the 25-μs simulation. Although acetylcholine quickly passed through the extracellular vestibule en route to the binding pocket, it did not exhibit metastable binding in the vestibule. Acetylcholine exhibited significant mobility in the binding pocket, likely reflecting the low affinity of the crystallized inactive state for agonists.

Forced dissociation of tiotropium

To identify the entire binding/dissociation pathway, we “pushed” tiotropium out of the binding pocket of both the M_2 and M_3 receptors[50,51]. Production simulations were initiated from configurations of the corresponding unbiased trajectory. These simulations employed a time-dependent harmonic biasing potential, $U(t)$:

$$U(t)=\frac{1}{2}k(d-d_0(t))^2$$

where t is time, k is a force constant in units of kcal/mol/A^2, d is the distance between the center-of-mass of the heavy atoms of tiotropium and the center-of- mass of the protein Cα atoms, and $d_0(t)$ varied linearly over 1.0 μs from 9.6 A to 33 A for M_2 and from 8.6 A to 32 A for M_3. This biasing term does not impose any preferred direction of ligand exit. We performed seven such simulations for each of M_2 and M_3,with k = 5, starting from configurations extracted from the tiotropium bound simulations of M_2 and M_3. Each initial configuration was separated in time by 36 ns. Results were similar across all simulations.

Force field parameters

The CHARMM27 parameter set[29] with CMAP terms[52] and a recently introduced correction to charged side-chain electrostatics[53] was used for all protein molecules and salt ions in conjunction with the CHARMM TIP3P[54] water model and a modified CHARMM lipid force field[55]. Force field parameters for tiotropium and QNB were obtained from the CHARMM ParamChem web server[56], version 0.9.1 beta. QNB was simulated in its protonated (ammonium) state. To evaluate the assigned partial charges assigned by ParamChem, we performed a quantum mechanical computation of the electrostatic potential at a collection of points surrounding each ligand (*in vacuo* at the HF/6-31G* level of theory using MOLPRO[57]), and compared it to the potential generated by the assigned charges.

Analysis protocols

Trajectory snapshots, each containing a record of all atom positions at a particular instant in time, were saved every 180 ps during production simulations. Distance measurements were computed using the HiMach parallel analysis framework[58]. VMD[59] was used to visualize trajectories and to produce Fig. 3a and Fig. 3b.

To determine the most common vestibule-bound poses of tiotropium shown in Fig. S4, we performed a clustering analysis on the 14.2-μs spontaneous binding simulation of M_2 (Table S4, condition D) and the 16.0-μs spontaneous binding simulation of M_3 (Table S4, condition E). We performed *k*-means clustering on the set of trajectory snapshots in which a tiotropium molecule was in the extracellular vestibule, using the positions of atoms indicated in Fig. S4c. Clusters representing highly similar poses were merged.

Supplementary Material

Refer to Web version on PubMed Central for supplementary material.

Acknowledgments

We acknowledge support from National Institutes of Health Grants NS028471 (B.K.K.), GM56169 (W.I.W.), and the Mathers Foundation (B.K.K. and W.I.W.), and from the National Science Foundation (A.C.K.). This work was supported in part by the Intramural Research Program, NIDDK, NIH, US Department of Health and Human Services (Bethesda, MD, USA). We thank Reinhard Grisshammer (NIH, NINDS, Rockville, MD) and Stefano Costanzi (NIH, NIDDK, Bethesday, MD) for advice and helpful discussions during various stages of the project, Yaru Zhou (NIH, NIDDK, Bethesda, MD) for carrying out radioligand binding assays with several M_3 receptor-T4 fusion constructs, Daniele Scarpazza (D. E. Shaw Research) for developing software that enabled forced dissociation simulations, and Andrew Taube, Kim Palmo, and David Borhani (D. E. Shaw Research) for advice related to simulations.

Literature cited

1. Loewi O. Uber humorale ubertragbarkeit der Herznervenwirkung. Pflugers Arch. 1921; 189:239–242.
2. Hulme EC, Birdsall NJM, Buckley NJ. Muscarinic receptor subtypes. Ann Rev Pharmacol and Toxicol. 1990; 30:633–673. [PubMed: 2188581]
3. Wess J. Molecular biology of muscarinic acetylcholine receptors. Crit Rev Neurobiol. 1996; 10:69–99. [PubMed: 8853955]
4. Caulfield MP, Birdsall NJM. International union of pharmacology. XVII Classification of muscarinic acetylcholine receptors. Pharmacol Rev. 1998; 50 :279–290. [PubMed: 9647869]

5. Conn PJ, Jones CK, Lindsley CW. Subtype-selective allosteric modulators of muscarinic receptors for the treatment of CNS disorders. Trends Pharmacol Sci. 2009; 30:148–155. [PubMed: 19201489]
6. Wess J, Eglen RM, Gautam D. Muscarinic acetylcholine receptors: mutant mice provide new insights for drug development. Nat Rev Drug Discov. 2007; 6:721–733. [PubMed: 17762886]
7. Yamada M, et al. Mice lacking the M_3 muscarinic acetylcholine receptor are hypophagic and lean. Nature. 2001; 410:207–212. [PubMed: 11242080]
8. Poulin B, et al. The M_3-muscarinic receptor regulates learning and memory in a receptor phosphorylation/arrestin-dependent manner. Proc Natl Acad Sci USA. 2010; 107:9440–9445. [PubMed: 20439723]
9. Gautam D, et al. Neuronal M_3 muscarinic acetylcholine receptors are essential for somatotroph proliferation and normal somatic growth. Proc Natl Acad Sci USA. 2009; 106:6398–6403. [PubMed: 19332789]
10. Wess J, Han SJ, Kim SK, Jacobson KA, Li JH. Conformational changes involved in G-protein-coupled-receptor activation. Trends Pharmacol Sci. 2008; 29:616–625. [PubMed: 18838178]
11. Rosenbaum DM, et al. GPCR engineering yields high-resolution structural insights into beta2-adrenergic receptor function. Science. 2007; 318:1266–1273. [PubMed: 17962519]
12. Haga K, et al. Structure of the human M2 muscarinic acetylcholine receptor bound to an antagonist. Nature. 2012; XXX:YYY–ZZZ.
13. Scarselli M, Li B, Kim SK, Wess J. Multiple residues in the second extracellular loop are critical for M_3 muscarinic acetylcholine receptor activation. J Biol Chem. 2007; 282:7385–7396. [PubMed: 17213190]
14. Barnes PJ. The pharmacological properties of tiotropium. Chest. 2000; 117:63S–66S. [PubMed: 10673478]
15. Casarosa P, Kiechle T, Sieger P, Pieper M, Gantner F. The constitutive activity of the human muscarinic M_3 receptor unmasks differences in the pharmacology of anticholinergics. J Pharmacol Exp Ther. 2010; 333:201–209. [PubMed: 20035022]
16. Bolden C, Cusack B, Richelson E. Antagonism by antimuscarinic and neuroleptic compounds at the five cloned human muscarinic cholinergic receptors expressed in Chinese hamster ovary cells. J Pharmacol Exp Ther. 1992; 260:576–580. [PubMed: 1346637]
17. Ballesteros JA, Weinstein H. Integrated methods for the construction of three-dimensional models and computational probing of structure-function relations in G protein coupled receptors. Meth Neurosci. 1995; 25:366–428.
18. Li B, et al. Rapid identification of functionally critical amino acids in a G protein-coupled receptor. Nat Methods. 2007; 4:169–174. [PubMed: 17206152]
19. Lebon G, Langmead CJ, Tehan BG, Hulme EC. Mutagenic mapping suggests a novel binding mode for selective agonists of M_1 muscarinic acetylcholine receptors. Mol Pharmacol. 2009; 75:331–341. [PubMed: 19001633]
20. Drubbisch V, Lameh J, Philip M, Sharma YK, Sadee W. Mapping the ligand binding pocket of the human muscarinic cholinergic receptor Hm1: Contribution of Tyrosine-82. Pharm Res. 1992; 9:1644–1647. [PubMed: 1488411]
21. Dror RO, et al. Pathway and mechanism of drug binding to G-protein-coupled receptors. Proc Natl Acad of Sci USA. 2011; 108:13118–13123. [PubMed: 21778406]
22. Redka, DyS; Pisterzi, LF.; Wells, JW. Binding of orthosteric ligands to the allosteric site of the M_2 muscarinic cholinergic receptor. Mol Pharmacol. 2008; 74:834–843. [PubMed: 18552124]
23. Valant C, et al. A novel mechanism of G protein-coupled receptor functional selectivity. J Biol Chem. 2008; 283:29312–29321. [PubMed: 18723515]
24. Wong SKF. G protein selectivity is regulated by multiple intracellular regions of GPCRs. Neurosignals. 2003; 12:1–12. [PubMed: 12624524]
25. Blin N, Yun J, Wess J. Mapping of single amino acid residues required for selective activation of G_q by the M_3 muscarinic acetylcholine receptor. J Biol Chem. 1995; 270:17741–17748. [PubMed: 7629074]
26. Liu J, Conklin BR, Blin N, Yun J, Wess J. Identification of a receptor/G-protein contact site critical for signaling specificity and G-protein activation. Proc Natl Acad Sci USA. 1995; 92:11642–11646. [PubMed: 8524820]

27. Rasmussen SGF, et al. Crystal structure of the β_2 adrenergic receptor-Gs protein complex. Nature. 2011; 477:549–555. [PubMed: 21772288]
28. Bluml K, Mutschler E, Wess J. Functional role of a cytoplasmic aromatic amino acid in muscarinic receptor-mediated activation of phospholipase C. J Biol Chem. 1994; 269:11537–11541. [PubMed: 8157684]
29. MacKerell AD, et al. All-atom empirical potential for molecular modeling and dynamics studies of proteins. J Phys Chem B. 1998; 102:3586–3616. [PubMed: 24889800]
30. Shaw, DE., et al. Proceedings of the Conference on High Performance Computing, Networking, Storage and Analysis; Portland, Oregon: ACM; 2009.
31. Kukkonen JP, Nasman J, Ojala P, Oker-Blom C, Akerman KE. Functional properties of muscarinic receptor subtypes Hm1, Hm3 and Hm5 expressed in Sf9 cells using the baculovirus expression system. J Pharmacol Exp Ther. 1996; 279:593–601. [PubMed: 8930161]
32. Chae PS, et al. Maltose-neopentyl glycol (MNG) amphiphiles for solubilization, stabilization and crystallization of membrane proteins. Nat Methods. 2010; 7:1003–1008. [PubMed: 21037590]
33. Caffrey M, Cherezov V. Crystallizing membrane proteins using lipidic mesophases. Nat Protoc. 2009; 4:706–731. [PubMed: 19390528]
34. Otwinowski, Z.; Minor, W. Meth Enzymol. Charles, W.; Carter, editors. Vol. 276. Academic Press; 1997. p. 307-326.
35. McCoy AJ, et al. Phaser crystallographic software. J Appl Crystallogr. 2007; 40:658–674. [PubMed: 19461840]
36. Adams PD, et al. PHENIX: a comprehensive Python-based system for macromolecular structure solution. Acta Cryst D. 2010; 66:213–221. [PubMed: 20124702]
37. Davis IW, Murray LW, Richardson JS, Richardson DC. MolProbity: structure validation and all-atom contact analysis for nucleic acids and their complexes. Nucleic Acids Res. 2004; 32:W615–W619. [PubMed: 15215462]
38. Schrodinger, LLC. The PyMOL Molecular Graphics System, Version 1.3r1. 2010.
39. Ward SD, Hamdan FF, Bloodworth LM, Wess J. Conformational changes that occur during M_3 muscarinic acetylcholine receptor activation probed by the use of an in situ disulfide cross-linking strategy. J Biol Chem. 2002; 277:2247–2257. [PubMed: 11698401]
40. Bonner TI, Buckley NJ, Young AC, Brann MR. Identification of a family of muscarinic acetylcholine receptor genes. Science. 1987; 237:527–532. [PubMed: 3037705]
41. Han SJ, et al. Pronounced conformational changes following agonist activation of the M_3 muscarinic acetylcholine receptor. J Biol Chem. 2005; 280:24870–24879. [PubMed: 15870064]
42. Dowling MR, Charlton SJ. Quantifying the association and dissociation rates of unlabelled antagonists at the muscarinic M_3 receptor. Br J Pharmacol. 2006; 148:927–937. [PubMed: 16847442]
43. Ellis J, Huyler J, Brann MR. Allosteric regulation of cloned m1-m5 muscarinic receptor subtypes. Biochem Pharmacol. 1991; 42:1927–1932. [PubMed: 1741770]
44. Dror RO, et al. Identification of two distinct inactive conformations of the β_2-adrenergic receptor reconciles structural and biochemical observations. Proc Natl Acad Sci USA. 2009; 106:4689–4694. [PubMed: 19258456]
45. Fahmy K, et al. Protonation states of membrane-embedded carboxylic acid groups in rhodopsin and metarhodopsin II: a Fourier-transform infrared spectroscopy study of site-directed mutants. Proc Natl Acad Sci USA. 1993; 90:10206–10210. [PubMed: 7901852]
46. Rosenbaum DM, et al. Structure and function of an irreversible agonist- β_2 adrenoceptor complex. Nature. 2011; 469:236–240. [PubMed: 21228876]
47. Krautler V, van Gunsteren WF, Hunenberger PH. A fast SHAKE algorithm to solve distance constraint equations for small molecules in molecular dynamics simulations. J Comput Chem. 2001; 22:501–508.
48. Tuckerman M, Berne BJ, Martyna GJ. Reversible multiple time scale molecular dynamics. J Chem Phys. 1992; 97:1990.
49. Shan Y, Klepeis JL, Eastwood MP, Dror RO, Shaw DE. Gaussian split Ewald: A fast Ewald mesh method for molecular simulation. J Chem Phys. 2005; 122:054101.

50. Grubmuller H, Heymann B, Tavan P. Ligand Binding: Molecular Mechanics Calculation of the Streptavidin-Biotin Rupture Force. Science. 1996; 271:997–999. [PubMed: 8584939]
51. Izrailev S, et al. Molecular dynamics study of unbinding of the avidin-biotin complex. Biophys J. 1997; 72:1568–1581. [PubMed: 9083662]
52. Mackerell AD Jr, Feig M, Brooks CL 3rd. Extending the treatment of backbone energetics in protein force fields: limitations of gas-phase quantum mechanics in reproducing protein conformational distributions in molecular dynamics simulations. J Comput Chem. 2004; 25:1400–1415. [PubMed: 15185334]
53. Piana S, Lindorff-Larsen K, Shaw DE. How robust are protein folding simulations with respect to force field Parameterization? Biophys J. 2011; 100:L47–L49. [PubMed: 21539772]
54. Beglov D, Roux B. Finite representation of an infinite bulk system: solvent boundary potential for computer simulations. J Chem Phys. 1994; 100:9050–9063.
55. Klauda JB, et al. Update of the CHARMM all-atom additive force field for lipids: validation on six lipid types. J Phys Chem B. 2010; 114:7830–7843. [PubMed: 20496934]
56. Vanommeslaeghe K, et al. CHARMM general force field: A force field for drug-like molecules compatible with the CHARMM all-atom additive biological force fields. J Comput Chem. 2010; 31:671–690. [PubMed: 19575467]
57. Werner, H-J., et al. MOLPRO, version 2010.1, a package of ab initio programs. Cardiff University; UK: 2010.
58. Tu, T., et al. Proceedings of the 2008 ACM/IEEE Conference on Supercomputing; Austin, Texas: IEEE Press; 2008.
59. Humphrey W, Dalke A, Schulten K. VMD: visual molecular dynamics. J Mol Graphics. 1996; 14:33–38.

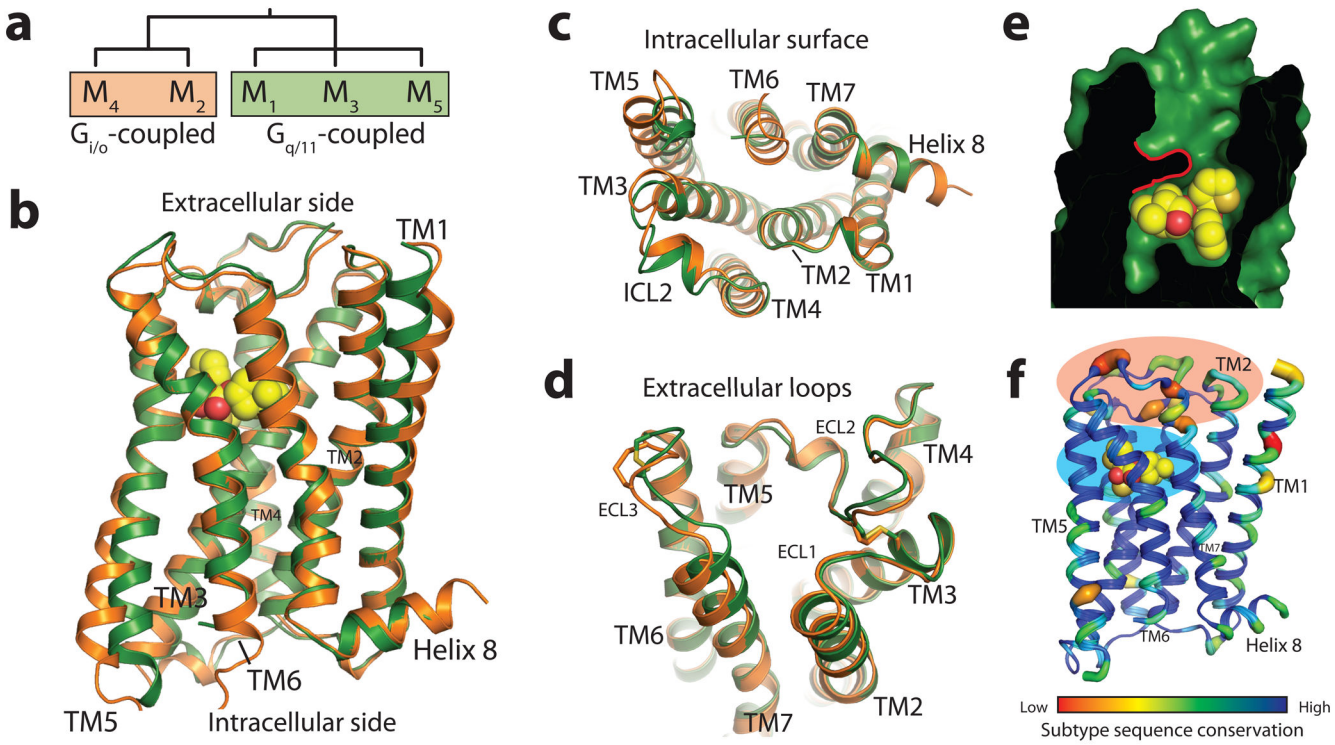

Figure 1. Major structural features of the M_3 receptor

a, Analysis of muscarinic receptor sequences divides them into two classes. **b**, The overall structure of the M_3 receptor (green) is similar to that of the M_2 receptor (orange). The M_3-bound ligand, tiotropium, is shown in spheres **c**, Comparison of the intracellular surfaces shows divergence in the cytoplasmic end of transmembrane helix 5. **d**, Comparison of the extracellular surfaces shows less deviation, with near perfect conservation of backbone fold of extracellular loops **e**, A solvent accessible surface for the M_3 receptor bound to tiotropium (spheres) shows the receptor covering the ligand with a tyrosine lid (outlined in red). **f**, M_3 receptor structure colored by sequence conservation among the five mAChR subtypes. Poorly conserved regions are shown with larger backbone diameter. The orthosteric and allosteric sites are indicated in blue and red, respectively, and the ligand tiotropium is shown in spheres.

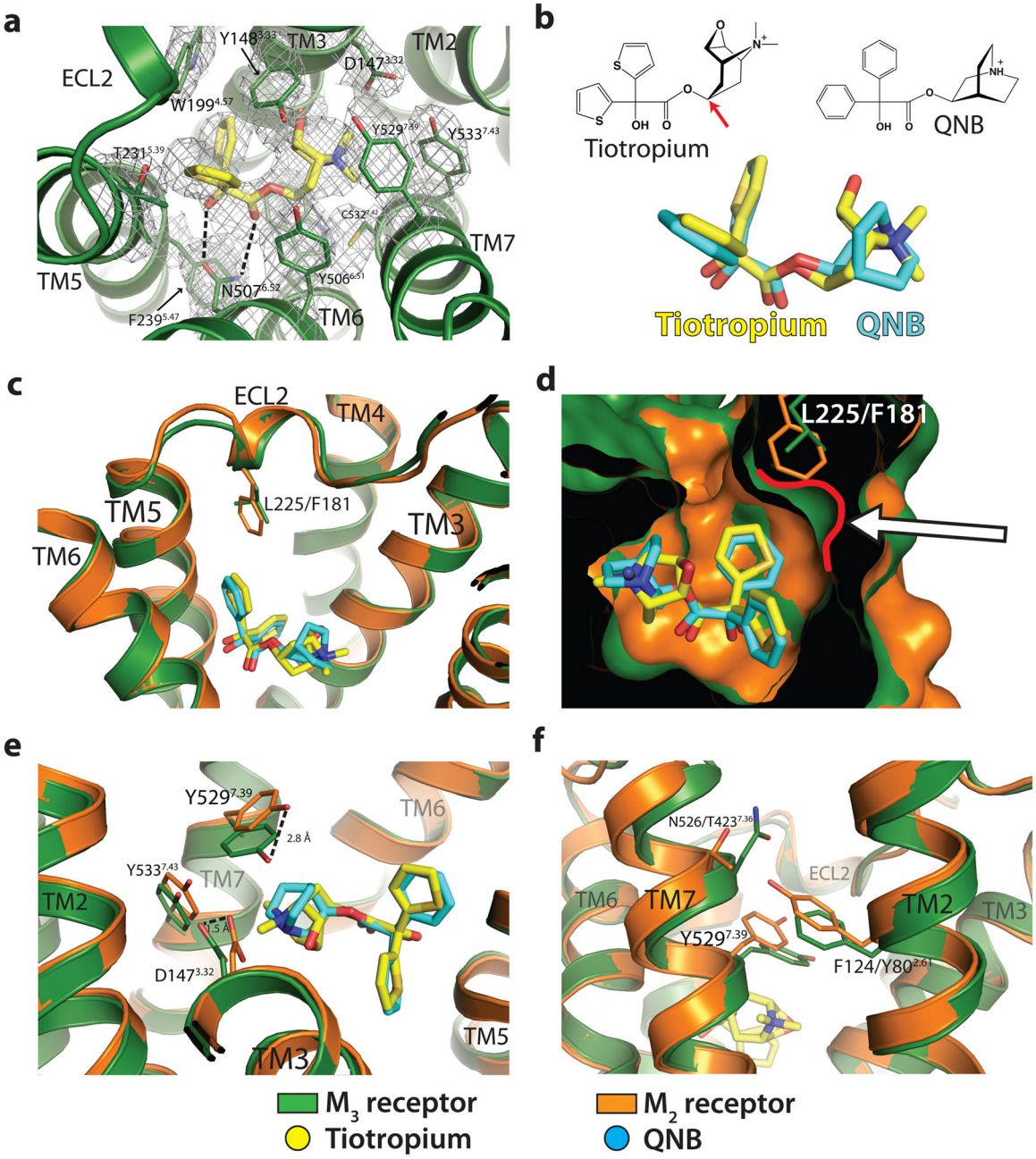

Figure 2. Orthosteric binding sites of the M_2 and M_3 receptors

In all panels, the M_3 receptor is green with its ligand tiotropium in yellow, while the M_2 receptor and its ligand QNB are shown in orange and cyan, respectively. **a**, Tiotropium binding site in the M_3 receptor. A $2F_o$-F_c map contoured at $2F_o$-F_c is shown in wire. **b**, Chemical structures of ligands. A red arrow indicates the tropane C3 atom used as a tracking landmark in Fig. 3. Superimposing the receptor structures reveals that the two ligands adopt highly similar poses (bottom). **c**, There is a Phe (M_2)/Leu (M_3) sequence difference between the M_2 and M_3 receptors near the binding site. **d**, This produces an enlarged binding pocket

in the M_3 receptor. **e**, A displacement of M_3 $Y529^{7.39}$ is seen. **f**, This may arise from a sequence difference at position 2.61 (Tyr80 in M_2 and Phe124 in M_3).

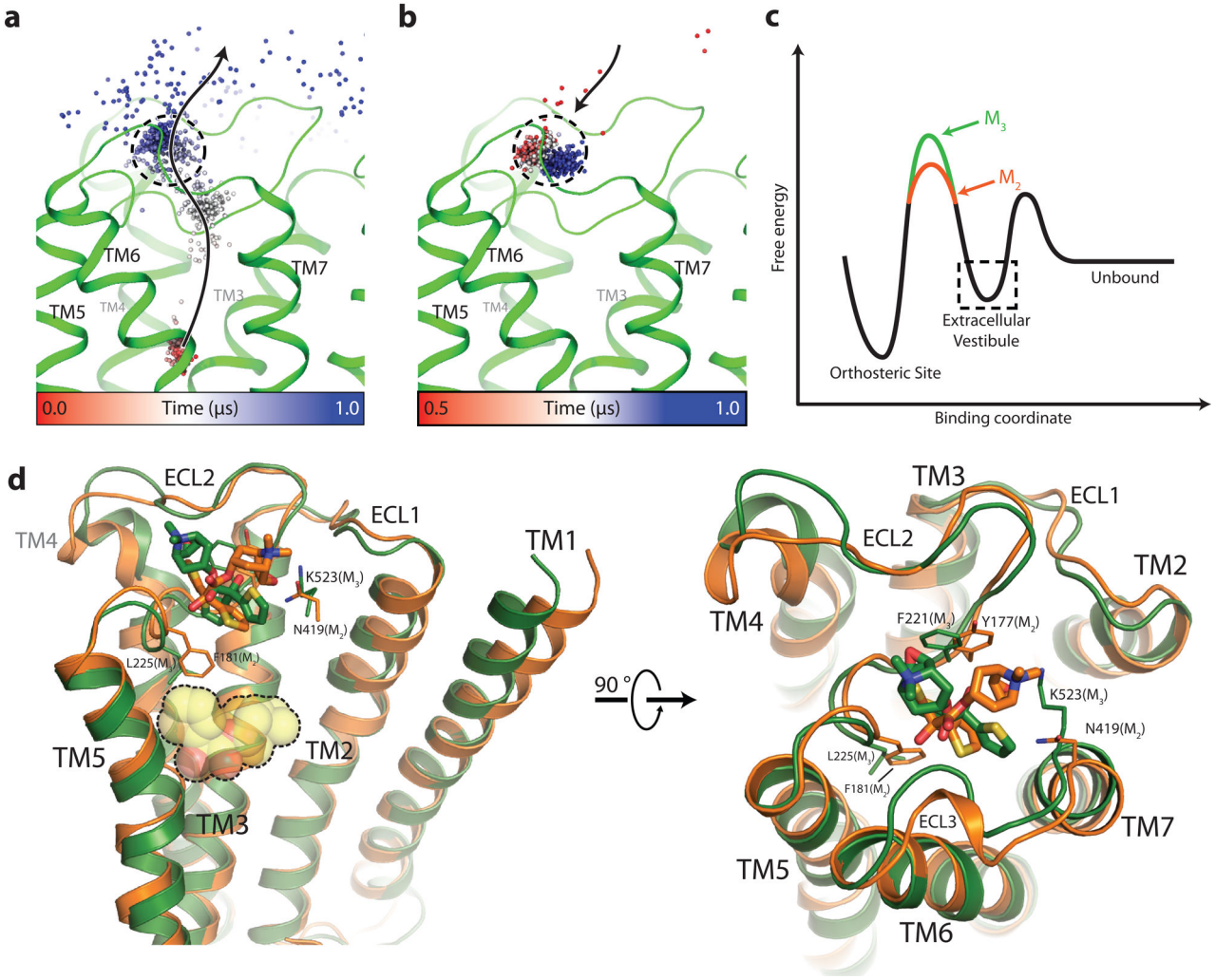

Figure 3. Molecular dynamics of ligand binding

Simulations suggest that the tiotropium binding/dissociation pathway for both receptors involves a metastable state in the extracellular vestibule. **a**, When tiotropium is pushed out of the binding pocket of M_3, it pauses in the extracellular vestibule. Spheres represent positions of the ligand's C3 tropane atom at successive points in time. **b**, When tiotropium is placed in solvent, it binds to the same site in the extracellular vestibule. Our simulations are insufficiently long for it to proceed into the orthosteric binding pocket; the agonist ACh, a much smaller molecule, bound spontaneously to the orthosteric site in similar simulations (see Supplementary Methods) **c,** Schematic free energy landscape for binding/dissociation. **d**, Common binding poses for tiotropium in the extracellular vestibule of M_2 (orange) and of M_3 (green). Non-conserved residues that contact the ligand are shown in thin sticks. The location of the orthosteric site is indicated by tiotropium in spheres.

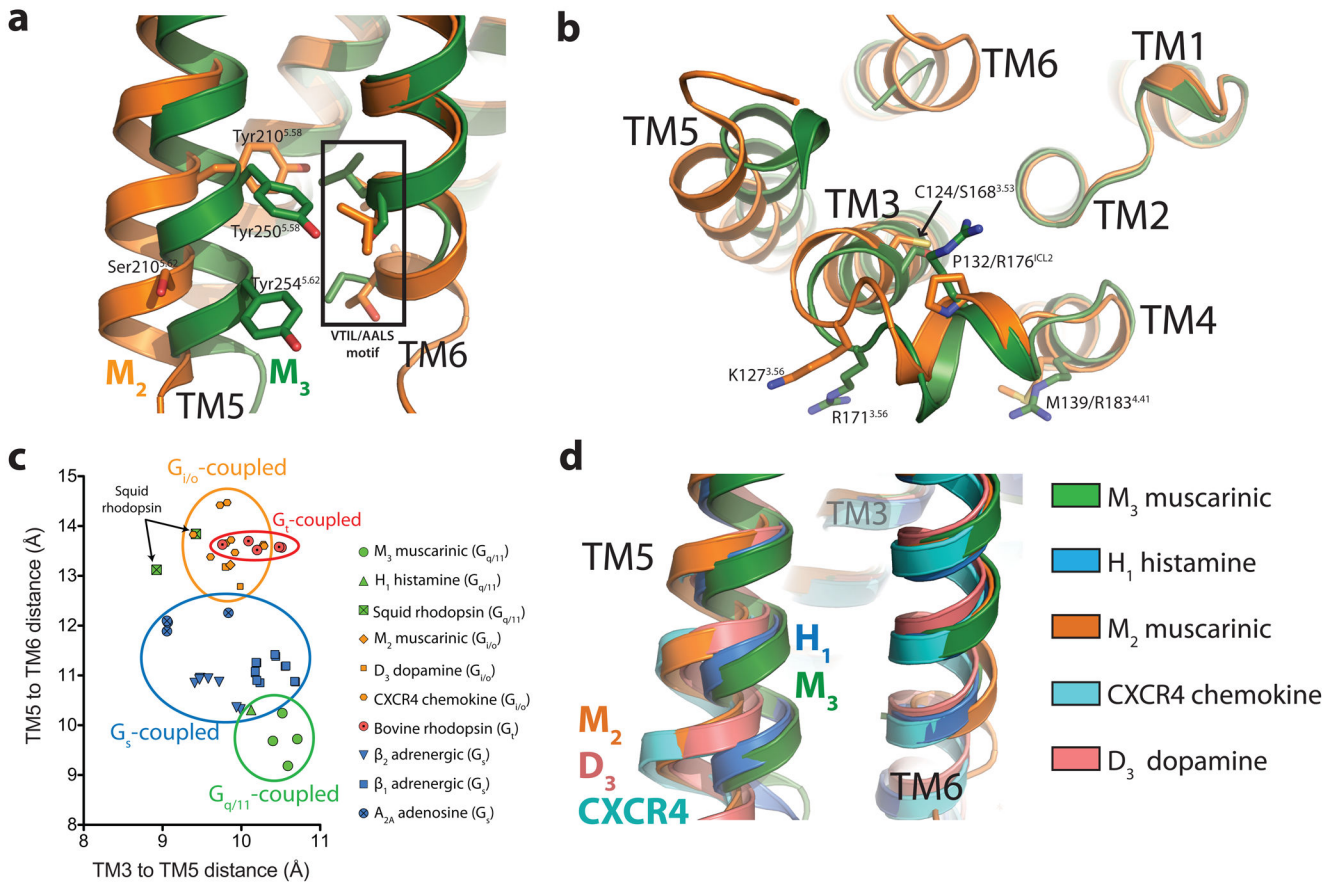

Figure 4. G protein coupling specificity determinants

a, The M_3 receptor shows displacement of TM5 relative to its position in M_2, and a conserved tyrosine (M_3 Tyr250$^{5.58}$) adopts different positions in the two receptors. Four TM6 residues near TM5 (AALS in M_3, VTIL in M_2) have been shown to be important coupling specificity determinants. **b**, ICL2 is also divergent between the two structures. Four residues previously implicated as specificity determinants[25] are shown, with residue numbers for M_2 followed by M_3 **c**, Plot of interhelical distances for crystallographically unique inactive GPCR structures published to date. Distances were measured between C_α atoms of TM5 residue 5.62 and TM3 residue 3.54 (x-axis), and TM5 residue 5.62 and TM6 residue 6.37 (y-axis). GPCRs cluster by coupling specificity, although squid rhodopsin is an exception. GPCRs coupling preferentially to $G_{i/o}$ and those coupling to the homologous G protein G_t cluster together. **d**, Structural alignment of mammalian $G_{i/o}$-coupled and $G_{q/11}$-coupled receptor structures.